Solid Earth Discuss., 7, 3689–3733, 2015
www.solid-earth-discuss.net/7/3689/2015/
doi:10.5194/sed-7-3689-2015

Solid Earth Discussions
Open Access
EGU

Studying local earthquakes in the northern Fennoscandian Shield using the data of the POLENET/LAPNET temporary array

O. A. Usoltseva[1] **and E. G. Kozlovskaya**[2,3]

[1]Institute of Geospheres Dynamics of the Russian Academy of Sciences, Leninsky Prospect, 38, building 1, 119334, Moscow, Russia
[2]Oulu Mining School, University of Oulu, P.O. Box 3000, 90014 Oulu, Finland
[3]Sodankylä Geophysical Observatory, University of Oulu, P.O. Box 3000, 90014 Oulu, Finland

Received: 19 November 2015 – Accepted: 23 November 2015 – Published: 8 December 2015

Correspondence to: O. A. Usoltseva (kriukova@mail.ru)

Published by Copernicus Publications on behalf of the European Geosciences Union.

Abstract

Earthquakes within areas inside continental plates are still not completely understood and the progress in understanding intraplate seismicity is slow due to short history of instrumental seismology and sparse regional seismic networks in seismically non-active areas. However, knowledge about position and depth of seismogenic structures in such areas is necessary, in order to estimate seismic hazard for such critical facilities as nuclear power plants and nuclear waste deposits. In the present paper we address the problem of seismicity in the intraplate area of northern Fennoscandia using the information on local events recorded by the POLENET/LAPNET temporary seismic array during the International Polar Year 2007–2009. We relocate the seismic events by the program HYPOELLIPS and grid search method. We use the first arrivals of P-waves of local events in order to calculate a 3-D tomographic P-wave velocity model of the uppermost crust (down to 20 km) for selected region inside the study area and show that the velocity heterogeneities in the upper crust correlate well with known tectonic units. We compare position of the velocity heterogeneities with the seismogenic structures delineated by epicentres of relocated events and demonstrate that these structures generally do not correlate with the crustal units formed as a result of crustal evolution in Archean and Paleoproterozoic. On the contrary, they correlate well with the post-glacial faults located in the area of the Baltic–Bothnia Megashear (BBMS). Hypocentres of local events have depths down to 30 km. We also obtain focal mechanisms of two selected events with good data quality. Both focal mechanisms are of strike-slip type in which shift prevails over uplift. Our results demonstrate that Baltic–Bothnia Megashear is an important large-scale, reactivated tectonic structure that has to be taken into account in estimating seismic hazard in northern Fennoscandia.

SED

7, 3689–3733, 2015

1 Introduction

The northern Fennoscandia has always been considered as an area of intraplate seismicity, with moderate-to-low seismic activity. Due to this, the story of instrumental seismology in the area is short and the present-day network of permanent seismic stations in the region is still not dense enough. That is why the progress on understanding where and when the earthquakes in the region may occur has been slow. Such areas are often considered as potentially attractive for such critical facilities as nuclear power plants, nuclear waste deposits and underground mines, for which proper seismic hazard estimates are required. Hence studying of local seismicity in intraplate areas benefits from deployment of dense temporary networks, like SVEKALAPKO (Bruneton et al., 2004; Hjelt et al., 2006; Sandoval et al., 2003, 2004). A new opportunity for investigating of intraplate seismicity in Fennoscandia was provided by the POLENET/LAPNET project.

POLENET/LAPNET was a sub-project of the multidisciplinary POLENET consortium (http://www.oulu.fi/sgo-oty/lapnet) related to seismic studies in the Arctic during the International Polar Year 2007–2009. The POLENET/LAPNET temporary seismic array was deployed in northern Fennoscandia (Finland, Sweden, Norway, and Russia). The array consisted of 35 temporary and 21 permanent seismic stations (Fig. 1a). Most of the stations of the array were equipped with broadband three-component sensors. The array registered waveforms of teleseismic, regional and local events from May 2007 to September 2009. The POLENET/LAPNET project became possible due to close cooperation of 12 organizations from 9 countries (see the list of organizations in Acknowledgements).

The northern part of the Fennoscandian shield is a region where the main part of the Earth crust was formed during Precambrian (Fig. 1b). The Paleoproterozoic (2.5–1.6 Ga) is the most important crust-forming period there. The Paleoproterozoic evolution of the shield can be divided into several major rifting and orogenic stages. The earlier Proterozoic events in the northern Fennoscandian shield are rifting of the Archean crust between 2.5 and 2.1 Ga, and consequent drifting and separation of the cratonic

SED
7, 3689–3733, 2015

components by newly formed oceans (Lahtinen et al., 2008). During the later Paleoproterozoic, 1.95–1.8 Ga, the fragments of previously dispersed Archaean crust were partly reassembled, which resulted in formation of the collisional orogen. The region of our study (Fig. 1, Region 1) comprises non-reworked part of the Archean Karelian craton and the part reworked in the Proterozoic (Daly et al., 2006). The area is cut by ancient shear zones (Berthelsen and Marker, 1986; Talbot, 2001) and numerous faults, stretching both from NE to SW, from NW to SE and from N to S.

According to previous studies (Wu et al., 1999; Arvidsson, 1996), the local seismicity in northern Fennoscandia can be explained by two factors: a post-glacial rebound and spreading in the Mid Atlantic Ridge (Hess, 1962). According to Nocque et al. (2005), the maximum vertical velocities in the post-glacial uplift area are observed at 22.5° E/64.6° N. In our study region the vertical uplift rate is approximately 6 mm yr^{-1}. The post-glacial faults in Fennoscandia are relatively recent faults formed after the last deglaciation. They are usually several dozen kilometres long with large fault displacements (Muir Wood, 1993; Bungum and Lindholm, 1996).

The structure of the crust and upper mantle of the Fennoscandian shield is very complex. It has been studied by different active and passive seismic experiments (Guggisberg, 1986; Guggisberg et al., 1991; Hauser and Stangl, 1990; Sharov, 1993; Luosto et al., 1989; Walther and Fluh, 1993; Kukkonen et al., 2006). Detailed 2-D *P* velocity models of upper crust along profiles in northern Fennoscandia were calculated in Silvennoinen et al. (2010) and Janik et al. (2009). Regional-scale 3-D P-wave velocity model of the crust for our region was calculated in Glaznev (2003), Pavlenkova (2006).

The data of the POLENET/LAPNET array was used in several studies aiming to obtain seismic velocity structure of the crust and upper mantle in northern Fennoscandia. A 3-D S-wave velocity model of the upper crust was obtained by ambient noise tomography (Poli et al., 2013). In Silvennoinen et al. (2014) the new map of the crust–mantle boundary was obtained for the POLENET/LAPNET study area using both previous controlled-source seismic profiles and P-wave receiver functions estimated for POLENET/LAPNET stations. Teleseismic P-wave velocity model of the upper mantle

SED
7, 3689–3733, 2015

beneath northern Fennoscandia was obtained by Silvennoinen et al. (2015) using teleseismic travel time tomography. The evidence of upper mantle seismic anisotropy was presented by Plomerova et al. (2011) and Vinnik et al.(2014).

The aim of the present paper is to obtain accurate coordinates of hypocentres of local events recorded by the POLENET/LAPNET array, delineate position and depth penetration of seismogenic structures and to obtain focal mechanisms of selected earthquakes. Another purpose of our study is to use the local events data in order to calculate a 3-D tomographic model of the uppermost crust (down to 20 km) for selected region inside the POLENET/LAPNET study area and to obtain new information about structure of the crust there. Previously, local events recorded by the POLENET/LAPNET array were studied in Usoltseva et al. (2012). The present work is continuation of this previous study.

2 Data

The seismic stations of the POLENET/LAPNET array were installed in quiet sites. The average spacing between stations is equal to 70 km. The stations recorded continuous data with sampling rate varying from 50 to 100 sps. Waveforms were stored in the standard seismological miniSeed format (http://www.iris.edu/manuals/SEEDManual_V2.4.pdf) in RESIF data centre hosted at University Joseph Fourier (http://portal.resif.fr).

Initial information about origin time and hypocentre coordinates of local seismic events was obtained from the catalogue of Institute of Seismology of the University of Helsinki, hereafter HEL catalogue (www.seismo.helsinki.fi). According to the HEL catalogue, 9174 explosions and 234 earthquakes in northern part of Fennoscandian Shield occurred during the POLENET/LAPNET data acquisition period. The majority of explosions originated from known quarries, for example one large cluster of epicentres is around 67.8° N and 25.5° E, while the other smaller cluster is around 67.5° N. and 22.0° E. In our study we used a set of local earthquakes and explosions recorded by

SED
7, 3689–3733, 2015

more than 6 stations of the array. Epicentres of these events are shown in Fig. 2. The seismic waveforms were reviewed with the Seismic Handler (SHM) program package (Stammler, 1993, http://www.seismic-handler.org/portal). Recordings were band-pass filtered with corner frequencies at 1 and 15 Hz and amplitude-normalized. Examples of seismograms (Z component) of two local events with different focal depth and one local explosion are shown in Fig. 3a–c.

As can be seen, arrivals of P-waves are present at offsets of 25–232 km. Shallow local earthquake with magnitude ML 2.2 and deep earthquake with magnitude ML 1.6 have distinct P- and S-wave arrivals, particularly at the short offsets (Fig. 3a and b). The local explosion (Fig. 3c) with ML = 1.1 has less distinct first arrival of S-wave. For deep earthquake we observe strong S-wave arrivals and weak P-wave arrivals at distances less than 100 km from the epicentre. The same tendency for amplitudes of the first arrivals of P- and S-waves was noticed by (Arvidsson et al., 1992) for Skovde earthquake with ML of 4.5. The strongest earthquake took place on 19 January 2008 at 19:52 UTC (67.23° N 23.80° E, dep = 10.4 km, ML = 2.2, HEL).

3 Picking of travel times of P-waves

As shown by Majdanski et al. (2007), the reliable recognition of different phases of body waves propagating through a 3-D structure and picking of their arrivals requires calculation of theoretical travel times using some a-priori known velocity model.

In our study we used the 1-D velocity model of the HUKKA-S profile (Fig. 1b) published by Janik et al. (2009). The original model consists of 6 layers in the crust and 2 layers in upper mantle. In our work we use a simplified version of this model, in which velocities in each layer are constant (Table 1). At initial stage the trajectories of direct and refracted seismic rays were calculated using the Snell's law.

Propagation of P-wave rays through the velocity model (Table 1) is shown in Figs. 4 and 5 for shallow and deep earthquakes, respectively, at offsets of 20–250 km. Minimal travel time corresponds to direct rays for a shallow earthquake at offsets less than

SED
7, 3689–3733, 2015

200 km. In this case the take-off angles are always less than 90°. For a deep earthquake the first arrivals of P-waves correspond to the direct waves at short distances and the waves refracted at the Moho boundary at long distances. Therefore the travel times of the first arrivals depend on the velocity structure of the upper crust for shallow earthquakes and of the whole crust and upper mantle for deep earthquakes. This is important both for focal mechanisms evaluation and for local events tomography. Accurate information about velocities in the upper 5 km of the crust is necessary for more accurate determination of hypocentres and focal mechanisms.

For shallow earthquakes the confusion between different seismic phases (direct wave and the wave refracted at the C2 boundary, see Fig. 4) can occur at offsets of 50–100 km. For events with hypocentre depths of more than 20 km the waves refracted at the C1 and C2 boundaries are absent. For such events the confusion between different seismic phases may occur at offsets more than 170 km. Thus the erroneous determination of the first P-wave arrival is more probable for shallow earthquakes. In order to avoid such confusion we calculated theoretical travel times of direct and refracted P-waves for each event and stations using the model from Table 1. The calculated arrival times were marked in seismograms. After particular analysis of waveforms and calculated synthetic travel times we compiled a dataset of arrival times for each station (Fig. 1a) and for each event (Fig. 2). Then the synthetic travel-time curves with reduction velocity of 8 km s^{-1} were constructed for all possible waves from velocity model in Table 1 and for all events.

The arrival times were picked at seismograms of stations with distances less than 250 km from the epicentre. The quality of the picked arrival time depends on different factors, such as noise level at a particular station and human activity in the correspondent period of time. The picked first arrivals were compared with the theoretical travel-time curves. Examples of such comparison are presented in Figs. 4 and 5 (upper plots). As seen, some of the observed travel times deviate significantly from the theoretical curves. Therefore, more correct and stable location of events is necessary in order to decrease this deviation.

SED
7, 3689–3733, 2015

4 Relocation of events

For location of events we used two different methods. One of them is HYPOELLIPS (Lahr, 1989). This is an iteration method for minimization of the root-mean-square residuals (RMS) between observed and calculated travel times using solution of underdetermined system of linear equations. In HYPOELLIPS the residuals are weighted as a function of distance, azimuth and depend on data quality. Damping is used in order to ensure convergence. each iteration the damping is changed depending on the RMS value. For error estimation a 68 % joint spatial confidence ellipsoid is calculated for each hypocentre (Lahr, 1989). Two characteristics of this ellipsoid are used for analysis of location accuracy (Tables 2 and 3). This is the maximum horizontal axis of ellipsoid (g_er/0.53) and the maximum vertical axis of ellipsoid (v_er/0.53).

The other method is a grid search method (Nelson and Vidale, 1990), in which global minimization of the RMS difference between observed and calculated travel times is performed. In our study we used our own programming realization of the method. This grid search method is uniform for arbitrary complex velocity models and has the same computation time for 1-D and 3-D velocity models. Originally, minimization was performed using objective functions both in L_1 and L_2 norms. But for the final relocation we selected the L_2 norm because the L_2 norm provided more precise hypocentre coordinates during testing of inversion algorithms with the data of local explosions with known coordinates. The study area was gridded with 800 by 800 by 60 grid points (1 km spacing). The transformation between the spherical coordinate system of the Earth to the Cartesian grid was performed by short distance conversion. The method utilizes finite difference computation of the first arrival times (Podvin and Lecomte, 1991). In contrast to HYPOELLIPS, the residuals of travel times are used without weighting. The lower limit of the error in hypocentre determination is equal to the step of the grid (1 km). In our study we used the grid search method also in order to investigate stability of solution for hypocentre.

SED
7, 3689–3733, 2015

Initially we tried to use the HYPOELLIPS with the P-wave arrival times only and also with both P- and S-wave arrivals. The comparison of results showed, however, that hypocentres obtained with the P-wave arrivals only have the similar accuracy as the hypocentres obtained with both P- and S-wave arrivals. It can be explained mainly by higher quality of the first arrivals of P-waves. That is why we decided to use only the first P-wave arrivals for relocation. Analysis of the waveforms showed that the first P-wave arrival is usually sharp, but the secondary P- and S-wave arrivals cannot be easily distinguished.

The above described relocation methods were tested using local explosions from the Hukkavaara hill, for which coordinates of hypocentres are known with high precision (master events). Example of the Hukkavaara explosion with ML = 1.5 is presented in Fig. 6, in which event waveforms recorded by the temporary station LP53 and the permanent station HEF are shown. The distance between the explosion and the stations is equal to 59 km for LP53 and to 103 km for HEF. In seismograms we can see an acoustic signal that is one of the explosion indicators. In station LP53 the maximal amplitude of the acoustic signal is considerable larger than the maximal amplitude of the seismic signal. At offset of 103 km this amplitudes have similar values. Thus in our case the acoustic signal attenuates faster than the seismic one.

The results of testing are presented in Table 2. We found out that event coordinates obtained by both methods are almost identical and the differences in origin times vary from 0.2 to 0.4 s. The RMS is less than 0.5 s for both methods and hypocentre depths are close to zero.

Table 3 presents results of relocation of 34 events from Region 2 by both methods. Events from Table 3 were divided into four groups. The first group contains 10 events, for which the location was not stable. We assume that location is not stable if the difference between hypocentres depths obtained by two methods is more than 8 km or the error for the hypocentre depth obtained by the HYPOELLIPSE is more than 8 km. For the second group of 14 events we obtained stable hypocentre solutions and depths less than 20 km. The third group consists of three events with hypocentres near the

SED
7, 3689–3733, 2015

surface. Therefore, they are probably explosions. Hypocentres of the forth group of 7 events have stable solutions and depth of more than 20 km. The hypocentres of most of the natural events from Table 3 are deeper than the hypocentres presented in HEL catalogue. This difference can be explained by different velocity models used for events location.

The earthquakes from the group of deep events are also indicated as the deep ones in the HEL catalogue. After relocation the possible depth of them varies from 21.9 to 53.5 km. For deep events we can see that differences in hypocentre depths determined by both methods are less than 4.5 km, while differences in latitudes and longitudes are less than 0.04 and 0.08°, respectively. The RMS error is less than 0.37 s. The minimal angle between two neighbouring stations (the gap) varies from 63 to 232°. The hypocentres of deep earthquakes are located in an elongated N–S oriented area. Comparison of calculated and observed travel times before and after relocation is presented in Fig. 7 for one selected deep event. Before relocation many residuals were larger than 1 s and after relocation all the residuals became smaller than 0.2 s. The seismograms for this event are presented in Fig. 3b. The correspondent spectrogram for the nearest station LP61 (the offset equal to 70 km after relocation) is presented in Fig. 8. The frequency of seismic signal varies from 2 to 35 Hz. The duration of oscillations is 10 s in low frequencies and 40 s in high frequencies.

For groups of shallow earthquakes and explosions the accuracy of depth determination is lower than that for the group of deep events. It can be explained by higher probability of erroneous phase determination for surface events at large distances from the epicentre. The comparison of the observed and theoretical travel times before and after relocation is shown in Fig. 9 for one selected shallow earthquake. The correspondent seismograms are presented in Fig. 3a. The small difference between new and old residuals suggests that the quality of hypocentres in the Helsinki catalogue is satisfactory for the similar events from this region.

SED
7, 3689–3733, 2015

5 Focal mechanisms of selected events

For determination of focal mechanisms we used the program HASH (Hardebeck and Shearer, 2008), that estimates earthquake focal mechanisms from the first-motion polarities. We assumed that the earthquake source can be considered as a point source with a double-couple mechanism and that the rupture dimension in the source is much smaller than the distance to the stations and the wave length considered. The velocity model presented in Table 1 was used to determine take-off angles. The program HASH performs grid search over all possible values of strike, dip and rake angles. The polarity of signals at all stations was tested using strong teleseismic events. For visualization of focal mechanism solutions we used the software from "Computer programs in seismology" (Herrmann and Ammon, 2002).

We determined focal mechanisms of two earthquakes from P-wave first motion polarities. One of the earthquakes is the shallow event with ML = 1.9, the other one is the deep event with ML = 2.0 (Fig. 2). For the computation we used parameters of hypocentres determined by HYPOELLIPSE (Table 4). Results of focal mechanism calculations are presented in Table 4.

For the shallow event the data used consists of 18 first motion polarities. Signals corresponding to compressions are observed at 9 stations, from which 8 are impulsive and 1 is emergent. Signals corresponding to dilatations are observed at 9 stations, from which 8 are impulsive and 1 is emergent. For the deep event the data used consists of 12 first motions. Compressions are observed at 3 stations, including 2 impulsive signals and 1 emergent one, and dilatations are observed at 9 stations, including 7 impulsive signals and 2 emergent. The seismograms for shallow event showing the first motions are presented in Fig. 10. In Fig. 11 one can see lower hemisphere equal area projections of the focal sphere for researching events.

As follows from the dip value for both events, the hanging walls of both faults are close to the vertical. For Event 1 (the shallow one) the direction of the fault plane deviating 10–20° from the N–S direction clockwise is most likely. The focal mechanism

SED
7, 3689–3733, 2015

for Event 2 is probably corresponding to some fault stretching in longitude direction or with faults stretching NNE–SSW. Both focal mechanisms are of strike-slip type in which shift prevails over uplift. According to the rake angle obtained for the Event 1, the displacement of the western wall was in northern direction with respect to the eastern wall (right lateral movement). The rake angle obtained for the Event 2 suggests that it is possible that either the displacement of the eastern wall was in northern direction (left lateral) or the displacement of the northern wall was in NNE direction (right lateral).

6 Local events tomography

Local event tomography was used for estimating the P-wave velocity structure in the upper crust of our study region. The procedure consists of two steps. The first one is improvement of the a-priory 1-D model (Table 1) and calculating station corrections using the program VELEST (Kissling, 1988; Kissling et al., 1994) and the known hypocentre parameters. The second part incorporates simultaneous inversion for the 3-D velocity model and hypocentres coordinates using the SIMULSPS14 program (Thurber, 1983; Eberhart-Phillips, 1993; Thurber, 1993). In this code the raytracing is performed by shooting method of Virieux et al. (1988), where the ray connecting station and receiver in the given velocity model is found by varying the initial azimuth and take-off angle at the source. The 3-D velocity model is parameterized by regular grid. In the present study the distance between adjacent nodes equals 50 km in x direction and 30 km in y direction. Inversion is performed by damped least-squares method and resolution matrix is estimated simultaneously. The calculations were performed both with synthetic and real data.

As a starting model, we used the velocity model from Table 1. In modelling with VELEST we used 624 rays: 311 direct and 313 refracted ones. The number of observations for each station varies from 1 to 37. The RMS residuals for all events are decreased by 8 % after the third iteration. The velocities were modified only in the layers between 1.3 and 18 km and between 18 and 37 km. Final velocity values in these

SED
7, 3689–3733, 2015

layers are presented in Table 5. The station corrections are presented in Fig. 12 for the stations that registered more than 10 observations of the first arrival of P-wave. The maximum number of arrivals was observed at the permanent station HEF. That is why it was selected as a reference station. As seen from Fig. 12, the negative time corrections prevail in the northern part of the area, while in the South-East the positive time corrections are observed. Generally, the values and the signs of the station correction correlate with topography. Negative corrections were obtained for stations located at sites with large elevation (for example, KTK1 with elevation of 365 m or LAN with elevation of 500 m). In contrast, the stations installed at sites with low altitudes (for example, LP21 with elevation of 94 m or LP31 with elevation of 139 m) have positive station corrections. Exceptions are connected with the edge effects, for example, the station NIK situated near western boundary of the studied region has the elevation of 300 m and simultaneously the large positive correction.

The resolution was analysed through several checkerboard tests. The synthetic checkerboard velocity model was calculated by varying the velocity as a sinusoidal function in the x and y directions with a wavelength larger than the distance between two adjacent nodes of the grid. The maximum amplitude of positive and negative velocity perturbations was 6 % with respect to a background velocity model (Tables 1 and 5). Because of small amount of local events in our area it was necessary to evaluate the minimal size of heterogeneities that could be reconstructed. Therefore we perform synthetic tests with the cells of 75 km × 75 km, 100 km × 100 km and 150 km × 150 km (Fig. 13a–c, respectively). As the geological terrains in the study area (Fig. 1b) have generally elongated form, we performed also a resolution test with anomalies of 150 km × 75 km (Fig. 13d). Resolution test was performed also for checkerboard inhomogeneities oriented at an angle of 30° counter clockwise from the North (Fig. 14). As can be seen, all heterogeneities are reconstructed nearly perfectly at depths down to 18 km in the central part of the model. At the periphery only the large-scale velocity anomalies are seen. All testing models are well resolved down to a depth of ∼ 18 km for Region 2 (Fig. 1) in the North and slightly worse in the South. As

SED
7, 3689–3733, 2015

seen from Fig. 13, the magnitudes of anomalies recovered are generally smaller than those in the synthetic models.

Results of inversion with real data and with different model parametrisation are presented in Fig. 15, in which the horizontal cross-sections of the final velocity model are shown for 1.3, 10 and 18 km depths. The deviations of P-wave velocities from the 1-D background velocity model (Table 1, Table 5) do not exceed ±5 %. From the Fig. 15 one can see a high velocity zone in the northern part of the study area that continues to a depth of about 10 km. High velocities are observed to the west of 24° E, while low velocities prevail to the east of it. Also the elongated low velocity area stretching NE–SW is seen in the western part of region around 67° N. This area becomes more contrast and more wide with depth. As seen from Fig. 15, the large-scale velocity anomalies do not depend on model parametrization.

7 Discussion and conclusions

In spite of low seismic activity during the POLENET/LAPNET data acquisition period, it was possible to obtain accurate and reliable coordinates of hypocentres for a number of local earthquakes and to calculate the focal mechanisms of two of them. We also reconstructed a 3-D P-wave velocity model of the upper crust of our study area down to a depth of about 18 km. Generally, our results provide new knowledge about processes that cause intraplate seismicity in the northern Fennoscandia.

As seen from the Fig. 15, the P-wave velocity anomalies in the area with the good resolution are smaller than ±5 % with respect to the initial velocity model. The lateral heterogeneities in the upper crust in our velocity model are show general good correlation with the surface geology and are in agreement with the 3-D S-wave velocity model obtained by Poli et al. (2013) by ambient noise tomography as well as with the 2-D P- and S-wave velocity models along the POLAR profile (Janik et al., 2009) and P-wave velocity model along the southern segment FIRE4 profile (Silvennoinen et al., 2010). The high velocity anomaly correlates partly with the 2.1 Ga Greenstones area

SED
7, 3689–3733, 2015

and partly with the Lapland Granulite terrane (Fig. 1). These units correspond to the high P- and S-wave velocity zones in the upper crust in the model by Janik et al. (2009). Poli et al. (2013) also detected the high S-wave velocity anomaly corresponding to this unit.

The low velocity anomaly in the southern part of our study area is observed in the range of depths from 0 to 5 km and it disappears at a depth of 10 km (Fig. 15). This anomaly correlates with the southern part of Lapland Granitoid complex (LGC) and Peräpohja Schist belt (Fig. 1). The LGC is seen as a low S-wave velocity anomaly in the model by Poli et al. (2013). Silvennoinen et al. (2010) calculated high-resolution P-wave tomographic velocity model discovered a highly reflective high velocity and high density body beneath the LGC with the upper boundary at a depth of 1–3 km. This feature revealed by high-resolution seismic survey is not seen in our model that was parameterized with large blocks. The low velocity anomaly located approximately at Finnish–Swedish boundary at a depth of 18 km does not correlate with any geological unit and might be an inversion artefact.

Comparison of velocity anomalies revealed by seismic tomography (Fig. 15) with position of hypocentres of earthquakes and post-glacial faults (Fig. 16) suggests that seismogenic structures in our study region do not correlate with the boundaries of geological units formed in Archean and during their subsequent reactivation in Proterozoic. However, they show good correlation with known post-glacial faults in the region and are generally concentrated in a broad N–S-directed zone running from the Bothnian Bay to the Atlantic Ocean. This zone coincides with the old Precambrian Baltic–Bothnia Megashear zone (BBMS) (Berthelsen and Marker, 1986), interpreted in (Lahtinen et al., 2003) as an old plate boundary.

Van Lanen and Mooney (2007) proposed that such ancient suture zones have a high probability of reactivation. They also showed that existence of deeply penetrating crustal faults is the major parameter that controls distribution of intraplate earthquakes in stable continental region of North America. The deepest earthquakes in our study area (from catalogue HEL see in Fig. 16, from Table 3 see in Fig. 17) are located along

SED
7, 3689–3733, 2015

the BBMS, although not all of them can be associated with known post-glacial faults. According to (Arvidsson, 1996) the deepest earthquakes from the Lansjärv fault and the Lainio–Suijavaar fault have focal depths of 34 and 37 km, respectively. In our research the seismic events at Lansjarv and Lainio–Suljavaara faults located in the BBMS area have the hypocentres depths up to 20 km. Such deep earthquakes have not been detected at the post-glacial faults outside the BBMS. Namely, Ahmadi et al. (2015) showed that the current earthquake activity of the post-glacial Pärvie fault system (northern Sweden) is concentrated at a depth of about 11.5 km. In accordance with (Juhlin and Lund, 2011) the post-glacial Burtrask fault (northern Sweden) is traced down to a depth of about 2–3 km.

Figure 17 summarizes the available fault plane solutions for the earthquakes in the area of BBMS. The information about sources of these earthquakes is presented in Table 4 (our study) and Table 6 (previous studies). As seen, all the focal mechanisms with exception of Event 4 (Table 6) have a pronounced strike-sleep faulting and shear movement component. This is in contrast with the conclusion made by (Arvidsson, 1996), who interpreted the most of North Fennoscandian earthquakes as signatures of progressive rapid rise of the land from the centre of post-glacial rebound (Nocque et al., 2005). Also in the world stress map 2008 (http://dc-app3-14.gfz-potsdam.de/pub/stress_maps/stress_maps.html) only thrust faults are presented in Northern Fennoscandia, which are typical for the process of rebound.

Recently, Steffen et al. (2014) showed that depth of the fault tip and angle of the fault plays an important role in reactivation of faults by deglaciation processes. They find that steeply dipping faults ($\sim 75^{\circ}$) can be activated after glacial unloading, and fault activity continues thereafter. This agrees with the results of our study that shows that seismicity in the BBMS occurs at the steeply dipping faults penetrating to a depth down to 30 km. This also explains why this activity continues nowadays.

Generally, our study shows that the BBMS is an important reactivated large-scale tectonic suture in northern Fennoscandian shield that extends to greater depths than

SED
7, 3689–3733, 2015

some known post-glacial faults. This is necessary to take into account in estimating seismic hazard in the area.

Acknowledgements. The POLENET/LAPNET working group members are Elena Kozlovskaya, Helle Pedersen, Jaroslava Plomerová, Ulrich Achauer, Eduard Kissling, Irina Sanina, Teppo Jämsén, Hanna Silvennoinen, Catherine Pequegnat, Riitta Hurskainen, Robert Guiguet, Helmut Hausmann, Petr Jedlicka, Igor Aleshin, Ekaterina Bourova, Reynir Bodvarsson, Evald Brückl, Tuna Eken, Pekka Heikkinen, Gregory Houseman, Helge Johnsen, Elena Kremenetskaya, Kari Komminaho, Helena Munzarova, Roland Roberts, Bohuslav Ruzek, Hossein Shomali, Johannes Schweitzer, Artem Shaumyan, Ludek Vecsey and Sergei Volosov.

References

Ahmadi, O., Juhlin, C., Ask, M., and Lund, B.: Revealing the deeper structure of the end-glacial Pärvie fault system in northern Sweden by seismic reflection profiling, Solid Earth, 6, 621–632, doi:10.5194/se-6-621-2015, 2015.

Amante, C. and Eakins, B. W.: ETOPO1 1 Arc-Minute Global Relief Model: Procedures, Data Sources and Analysis, NOAA Technical Memorandum NESDIS NGDC-24, National Geophysical Data Center, NOAA, doi:10.7289/V5C8276M, 2009.

Arvidsson, R.: Fennoscandian earthquakes: whole crustal rupturing related to postglacial rebound, Science, 274, 744–746, doi:10.1126/science.274.5288.744, 1996.

Arvidsson, R., Wahlstrom, R., and Kulhanek, O.: Deep-crustal earthquakes in the southern Baltic Shield, Geophys. J. Int., 108, 767–777, 1992.

Berthelsen, A. and Marker, M.: 1.9–1.8 Ga old strike-slip megashears in the Baltic Shield, and their plate tectonic interpretation, Tectonophysics, 128, 163–181, 1986.

Bruneton, M., Pedersen, H. A., Farra, R., Arndt, N. T., Vacher, P., Achauer, U., Alinaghi, A., Ansorge, J., Bock, G., Friederich, W., Grad, M., Guterch, A., Heikkinen, P., Hjelt, S. E., Hyvonen, T. L., Ikonen, J. P., Kissling, E., Komminaho, K., Korja, A., Kozlovskaya, E., Nevsky, M. V., Paulssen, H., Pavlenkova, N. I., Plomerova, J., Raita, T., Riznichenko, O. Y., Roberts, R. G., Sandoval, S., Sanina, I. A., Sharov, N. V., Shomali, Z. H., Tiikainen, J., Wieland, E., Wylegalla, K., Yliniemi, J., and Yurov, Y. G.: Complex lithospheric structure under the central Baltic Shield from surface wave tomography, J. Geophys. Res., 109, B10303, doi:10.1029/2003JB002947, 2004.

SED
7, 3689–3733, 2015

Bungum, H. and Lindholm, C.: Seismo- and neotectonics in Finnmark, Kola and the southern Barents Sea, part 2: Seismological analysis and seismotectonics, Tectonophysics, 270, 15–28, 1996.
Daly, J. S., Balagansky, V. V., Timmerman, M. J., and Whitehouse, M. J.: The Lapland-Kola orogen: palaeoproterozoic collision and accretion of the northern Fennoscandian lithosphere, in: European Lithosphere Dynamics, edited by: Gee, D. G. and Stephenson, R. A., Geol. Soc. London, Mem. Ser., 32, 579–598, 2006
Eberhart-Phillips, D.: Local earthquake tomography: earthquake source regions, in: Seismic Tomography: Theory and Practice, edited by: Iyer, H. M. and Hirahara, K., 1993.
Glaznev, V. N.: Complex Geophysical Models of the Fennoscandian Lithosphere, Apatity, 252 p., (in Russian), 2003.
Guggisberg, B.: Eine zweidimensionale refraktionsseismiche Interpretation der Geschwindigkeitstiefenstruktur des oberen Erdmantels unter dem Fennoskandischen Schild (Projekt FENNOLORA), PhD thesis, Eidg. Techn. Hochsch. Zurich, Zurich, Switzerland, 1986.
Guggisberg, B., Kaminski, W., and Prodehl, C.: Crustal structure of the Fennoscandian Shield: a traveltime interpretation of the long-range FENNOLORA seismic refraction profile, Tectonophysics, 195, 105–137, doi:10.1016/0040-1951(91)90208, 1991.
Hardebeck, J. L. and Shearer, P. M.: HASH: A FORTRAN Program for Computing Earthquake First-Motion Focal Mechanisms – v1.2 – 31 January, 17 p., available at: http://quake.wr.usgs.gov/research/software/#HASH, 2008.
Hauser, F. and Stangl, R.: The structure of the crust and the lithosphere in Fennoscandia derived from a joint interpretation of P- and S-wave data of the FENNOLORA refraction seismic profile, in: Sixth EGT Workshop: Data Compilation and Synoptic Interpretation, edited by: Freeman,R. and Mueller, S., Eur. Sci. Found., Strasbourg, France, 71–92, 1990.
Herrmann, R. B. and Ammon, C. J.: Computer programs in seismology – Source inversion, v.3–30, p. 98, 2002.
Hess, H. H.: History of ocean basins, in: Petrologic Studies: A Volume in Honor of A. F. Buddington, edited by: Engel, A. E. J., James, H. L., and Leonard, B. F., Geological Society of America, Boulder, CO, 599–620, 1962.
Hjelt, S.-E., Korja, T., Kozlovskaya, E., Lahti, I., Yliniemi, J., and BEAR and SVEKALAPKO Working Groups: Electrical conductivity and seismic velocity structures of the lithosphere

SED
7, 3689–3733, 2015

beneath the Fennoscandian Shield, in: European Lithosphere Dynamics, edited by: Gee, D., and Stephenson, R., Geol. Soc. London, Mem. Ser., 32, 2006.
Janik, T., Kozlovskaya, E., Heikkinen, P., Yliniemi, J., and Silvennoinen, H.: Evidence for preservation of crustal root beneath the Proterozoic Lapland-Kola orogen (northern Fennoscandian shield) derived from P and S wave velocity models of POLAR and HUKKA wide-angle reflection and refraction profiles and FIRE4 reflection transect, J. Geophys. Res., 114, B06308, doi:10.1029/2008JB005689, 2009.
Juhlin, C. and Lund, B.: Reflection seismic studies over the end-glacial Burträsk fault, Skellefteå, Sweden, Solid Earth, 2, 9–16, doi:10.5194/se-2-9-2011, 2011.
Kissling, E.: Geotomography with local earthquake data, Rev. Geophys., 26, 659–698, doi:10.1029/RG026i004p00659, 1988.
Kissling, E., Ellsworth, W. L., Eberhart-Phillips, D., and Kradolfer, U.: Initial reference models in local earthquake tomography, J. Geophys. Res., 99, 635–646, 1994.
Koistinen, T., Stephens, M. B., Bogatchev, V., Nordgulen, Ø., Wennerström, M., and Korhonen, J.: Geological map of Fennoscandian shield, scale 1 : 2 000 000, Geological Surveys of Finland, Norway and Sweden and the North-West Department of Natural Resources of Russia, 2001.
Kukkonen, I. T., Heikkinen, P., Ekdahl, E., Hjelt, S.-E., Yliniemi, J., Jalkanen, E., and FIRE Working Group: Acquisition and geophysical characteristics of reflection seismic data on FIRE transects, Fennoscandian Shield, in: Finnish Reflection Experiment (FIRE) 2001–2005, edited by: Kukkonen, I. T. and Lahtinen, R., Geol. Surv. of Finland, Espoo, Finland, 13–44, 2006.
Lahr, J. C.: HYPOELLIPSE/Version 2.0: A computer program for determining local earthquake hypocentral parameters, magnitude, and first motion pattern, U.S. Geological Survey Open-File Report 89–116, p. 92, 1989.
Lahtinen, R., Korja, A., and Nironen, M.: Paleoproterozoic tectonic evolution, in: Precambrian Geology of Finland – Key to the Evolution of the Fennoscandian Shield, edited by: Lehtinen, M., Nurmi, P. A., and Ramo, O. T., Elsevier Science, Amsterdam, 481–531, 2005.
Lahtinen R, Garde, A. A., and Melezhik, V. A.: Paleoproterozoic tectonic evolution of Fennoscandia and Greenland, Episodes, 31, 1–9, 2008.
Luosto, U., Flueh, E. R., Lund, C.-E., and Working Group: The crustal structure along the POLAR Profile from seismic refraction investigation, Tectonophysics, 162, 51–85, doi:10.1016/0040-1951(89)90356-9, 1989.

SED
7, 3689–3733, 2015

Majdanski, M., Kozlovskaya, E., and Grad, M.: 3D structure of the Earth's crust beneath the northern part of the Bohemian Massif, Tectonophysics, 438, 57–77, 2007.
Muir Wood, R.: A Review of the Seismotectonics of Sweden, Rep., 43-01-R-001 for Svensk Karnbranslehandtering AB ŽSKB, Stockholm, 225, 1993.
Nelson, G. D. and Vidale, J. E.: Earthquake locations by 3-d finite-difference travel times, B. Seismol. Soc. Am., 80, 395–410, 1990.
Nocque, J.-M., Calais, E., and Parsons, B.: Geodetic constraints on glacial isostatic adjustment in Europe, GRL, 32, L06308, doi:10.1029/2004GL022174, 2005.
Pavlenkova, N. I.: Lithospheric structure of the Baltic shield from DSS data, in: Structure and Dynamics of the Lithosphere of Eastern Europe, Geokart, Geos, Moscow, Russia, 33–58, 2006.
Plomerová, J., Vecsey, L., Babuška, V., and LAPNET Working Group: Domains of Archean mantle lithosphere deciphered by seismic anisotropy – inferences from the LAPNET array in northern Fennoscandia, Solid Earth, 2, 303–313, doi:10.5194/se-2-303-2011, 2011.
Podvin, P. and Lecomte, I.: Finite difference computation of travel times in very contrasted velocity models: a massively parallel approach and its associated tools, Geophys. J. Int., 105, 271–284, 1991.
Poli, P., Campillo, M., Pedersen, H., and the POLENET/LAPNET Working Group: Noise directivity and group velocity tomography in a region with small velocity contrasts: the northern Baltic shield application to the northern Baltic Shield, Geophys. J. Int., 192, 413–424, doi:10.1093/gji/ggs034, 2013.
Sandoval, S., Kissling, E., Ansorge, J., and the SVEKALAPKO STWG: High-Resolution body wave tomography beneath the SVEKALAPKO array: I. A-priori 3D crustal model and associated travel time effects on teleseismic wavefronts, Geophys. J. Int., 153, 75–87, 2003.
Sandoval, S., Kissling, E., Ansorge, J., and the SVEKALAPKO STWG: High-resolution body wave tomography beneath the SVEKALAPKO array: II. Anomalous upper mantle structure beneath central Baltic Schield, Geophys. J. Int., 157, 200–214, 2004.
Sharov, N. V.: Lithosphere of the Baltic Shield Based on Seismic Data (in Russian), Kola Res. Cent., Apatity, Russia, 144 pp., 1993.
Silvennoinen, H., Kozlovskaya, E., Yliniemi, J., and Tiira, T.: Wide angle reflection and refraction seismic and gravimetric model of the upper crust in FIRE4 profile area, northern Finland, Geophysica, 46, 21–46, 2010.

SED
7, 3689–3733, 2015

Silvennoinen, H., Kozlovskaya, E., Kissling, E., Kosarev, G., and the POLENET/LAPNET Working Group: A new Moho boundary map for the northern Fennoscandian Shield based on combined controlled-source seismic and receiver function data, GeoResJ, 1–2, 19–32, 2014.

Silvennoinen, H., Kozlovskaya, E., and Kissling, E.: POLENET/LAPNET teleseismic P-wave traveltime tomography model of the upper mantle beneath northern Fennoscandia, Solid Earth Discuss., 7, 2527–2562, doi:10.5194/sed-7-2527-2015, 2015.

Stammler, K.: SeismicHandler – programmable multichannel data handler for interactive and automatic processing of seismological analyses, Computat. Geosciences, 19, 135–140, 1993.

Steffen, R., Steffen, H., Wu, P., and Eaton, D. W.: Stress and fault parameters affecting fault slip magnitude and activation time during a glacial cycle, Tectonics, 33, 1461–1476, doi:10.1002/2013TC003450, 2014.

Talbot, C. J.: Weak zones in precambrian Sweden, Geol. Soc. Sp., 186, 287–304, doi:10.1144/GSL.SP.2001.186.01.17, 2001.

Thurber, C. H.: Earthquake locations and three-dimensional crustal structure in the Coyote Lake area, central California, J. Geophys. Res., 88, 8226–8236, 1983.

Thurber, C. H.: Local earthquake tomography: velocities and Vp/Vs – theory, in: Seismic Tomography: Theory and Practice, edited by: Iyer, H. M. and Hirahara, K., 1993.

Uski, M., Hyvonen, T., Korja, A., and Airo, M.: Focal mechanisms of three earthquakes in Finland and their relation to surface faults, Tectonophysics, 363, 141–157, 2003.

Usoltseva, O., Kozlovskaya, E., Konstantinovskaya, N., and POLENET/LAPNET Working Group Team: Intraplate seismicity in northern Fennoscandia from data of the POLENET/LAPNET experiment, Proceedings of the 9th International Conference PROBLEMS OF GEOCOSMOS, edited by: Troyan, V. N., Semenov, V. S., and Kubyshkina, M. V., ISBN 978-5-9651-0685-1, CD disk, 8 October–12, Saint-Petersburg State University (SPBU), Saint-Petersburg, Russia, p. 176–181, 2012.

Van Lanen, X and Mooney, W. D.: Integrated geologic and geophysical studies of North American continental intraplate seismicity, in: Continental Intraplate Earthquakes: Science, Hazard and Policy Issues, edited by: Stein, S. and Mazotti, S., Geological Society of America Special Paper, 425, p. 101–112, doi:10.1130/2007.2425(08), 2007.

Vinnik, L., Oreshin, S., Makeyeva, L., Peregoudov, D., Kozlovskaya, E., and POLENET/LAPNET Working Group: Anisotropic lithosphere under the Fennoscandian shield from P receiver

SED
7, 3689–3733, 2015

functions and SKS waveforms of the POLENET/LAPNET array, Tectonophysics, 628, 2530–2539, 2014.
Virieux, J., Farra, V., and Madariaga, R.: Ray tracing in laterally heterogeneous media for earthquake location, J. Geophys. Res., 93, 6585–6599, 1988.
Walther, C. and Fluh, E. R.: The POLAR profile revisited: combined P- and S- wave interpretation, Precambrian Res., 64, 153–168, doi:10.1016/0301-9268(93)90073-B, 1993.
Wu, P., Johnston, P., and Lambeck, K.: Postglacial rebound and fault instability in Fennoscandia, Geophys. J. Int., 139, 657–670, 1999.

SED
7, 3689–3733, 2015

Table 1. 1-D P-wave velocity model.

layer (km)	Vp ($km\,s^{-1}$)
0–1.3	6.2
1.3–18	6.3
18–37	6.6
37–40	7.15
40–44	7.4
44–50	8.03
Upper 50	8.4

SED
7, 3689–3733, 2015

Table 2. Results of Hukkavaara blasts location with using of HYPOELLIPS method (index 1) and grid search method (index 2). Sec1/2 – final source time defined by HYPOELLIPS/by grid search method, lat1/2 (lon1/2) – final latitude (longitude) defined by HYPOELLIPS/by grid search method. Dep1/2 – depth defined by HYPOELLIPS/by grid search method, RMS1 – final HYPOELLIPS root-mean-square residual, RMS2 – final grid search method RMS, gap – minimal angle between two neighbouring stations, *N* –number of POLENET/LAPNET stations used, g_er – 0.53 × maximum horizontal axes of 68 % joint-confidence ellipsoid, v_er – 0.53 × vertical axe of 68 % joint-confidence ellipsoid, r_{min} – epicentre distance up to nearest station, r_{max} – epicentre distance up to farthest station.

Yy m dd	hh:mi	sec1/ sec2	lat ° N 1/2	lon ° E 1/2	dep (km) 1/2	RMS1 (s)	RMS2 (s)	Gap (deg)	*N*	g_er (km)	V_er (km)	r_{min} (km)	r_{max} (km)
08 08 24	12:30	1.0/0.6	67.95/67.95	25.80/25.82	0.0/0.5	0.27	0.32	47	18	0.3	1.5	58	268
08 08 29	11:00	0.5/0.1	67.93/67.93	25.84/25.84	0.0/0.5	0.33	0.35	47	19	0.7	2	25	179
07 08 16	08:00	0.3/0.1	67.94/67.93	25.82/25.82	0.1/0.5	0.48	0.29	117	7	0.6	3	59	208

SED
7, 3689–3733, 2015

Table 3. Results of events location with using of HYPOELLIPS method (index 1) and grid search method (index 2). The notations are as in Table 2.

yy.mm.dd	hh:mi	sec1/sec2	lat ° N 1/2	lon ° E 1/2	dep (km) 1/2	RMS(s)1	RMS(s)2	Gap (deg)	*N*	g_er (km)	v_er (km)	r_{min} (km)	r_{max} (km)
Events with non stability location													
070920	20:38	40.0/39.6	67.89/67.88	22.66/22.69	13.6/1.5	0.39	0.23	174	10	1.4	1.4	53.3	230.8
071013	15:29	2.7/2.5	67.69/67.69	24.76/24.79	1.1/8.5	0.24	0.20	64	15	0.4	33.3	18.8	205.1
071128	04:39	41.8/41.7	67.39/67.40	24.29/24.33	8.2/0.5	0.15	0.13	160	12	2.1	16.1	33.7	154.9
71128	04:14	44.6/44.6	67.39/67.39	24.31/24.35	3.2/0.5	0.23	0.20	159	12	0.8	17.1	33.5	154.2
071207	20:38	48.6/48.5	67.10/67.11	25.78/25.81	7.3/10.5	0.16	0.17	64	15	0.5	12.6	49.9	218.3
080830	04:48	49.4/49.1	67.73/67.73	22.77/22.79	9.7/14.5	0.19	0.19	75	15	2	8.4	44.4	191.7
081206	05:32	29.8/29.7	68.09/68.11	23.49/23.57	12.8/21.5	0.35	0.39	179	11	3.3	3.5	27	183.1
081023	18:41	9.8/9.2	67.64/67.65	22.17/22.15	3.8/12.5	0.37	0.23	56	14	0.7	28.9	46	202.3
090425	10:32	45.7/45.2	68.54/68.54	23.33/23.38	4.7/16.5	0.17	0.22	92	13	0.9	9.1	20	193.3
090504	22:45	44.7/44.6	67.40/67.42	23.52/23.53	0.0/0.5	0.27	0.19	45	16	1.4	10.1	7.8	197.9
Events with stability location													
Shallow earthquakes (depth less 20 km)													
070702	03:04	10.1/9.9	68.04/68.05	22.85/22.88	11.0/14.5	0.25	0.22	172	8	1.5	1.5	47.6	208.6
070716	22:43	0.4/−0.1	68.49/68.52	23.72/23.75	9.6/11.5	0.1	0.15	105	7	0.5	1	10	192.1
070917	01:50	41.4/41.0	68.41/68.42	23.29/23.31	12.2/16.5	0.19	0.28	108	11	0.4	0.6	15.5	199.9
080119	19:52	3.1/3.1	67.25/67.26	23.78/23.85	13.0/13.5	0.19	0.17	160	22	0.4	0.5	23.5	235
080420	18:31	18.8/18.9	66.92/66.93	23.62/23.65	15.5/14.5	0.14	0.10	210	9	0.9	2.7	38.6	166.1
080531	07:17	30.1/30.1	67.03/67.03	24.08/24.12	6.5/8.5	0.36	0.38	174	9	0.5	1.9	14.6	154.5
080607	11:33	22.4/21.8	68.83/68.85	23.66/23.68	5.6/12.5	0.16	0.41	59	14	1.3	4.2	26.4	218.5
080719	19:11	19.0/18.7	67.95/67.97	22.79/22.81	7.4/8.5	0.32	0.30	80	19	0.4	0.8	35.1	234.4
080913	07:21	10.7/10.3	68.20/68.21	23.79/23.78	9.8/13.5	0.15	0.29	47	21	0.4	1.5	23.5	202.1
090120	11:32	20.5/20.3	67.54/67.54	22.14/22.18	7.8/7.5	0.21	0.14	117	11	1.6	2.2	11	197.8
090207	09:39	8.2/8.0	67.39/67.39	23.51/23.53	7.2/10.5	0.14	0.13	81	10	1.3	1.5	8.9	180.8
090215	00:38	55.0/55.0	67.67/67.68	22.41/22.47	3.5/3.5	0.34	0.31	63	15	0.4	1	29	214.6
090401	23:51	46.4/46.1	67.09/67.10	25.78/25.78	2.0/0.5	0.22	0.24	64	13	0.3	3.9	8.7	171.6
090505	18:22	14.4/14.2	67.93/67.94	23.26/23.27	8.2/13.5	0.21	0.28	54	17	0.9	2	28.4	200.8
Probably explosions													
071112	03:37	31.2/31.2	66.67/66.68	25.86/25.86	0.0/0.5	0.27	0.24	56	15	0.8	6.5	8.9	195.6
080212	03:41	11.8/11.9	66.93/66.93	24.08/24.15	0.0/0.5	0.28	0.23	156	18	0.5	2.7	22.2	234.6
090411	03:23	16.5/16.2	67.14/67.14	25.84/25.85	0.0/0.5	0.25	0.28	60	18	0.2	3.8	13.4	202.8
Deep earthquakes (depth more 20 km)													
070609	02:52	41.6/41.2	68.76/68.79	23.13/23.14	51.8/53.5	0.42	0.15	119	8	0.7	2	44.8	209.6
071003	12:26	40.2/40.3	67.44/67.46	22.86/22.93	28.4/29.5	0.14	0.18	195	10	0.7	0.7	69.7	206
080326	10:55	36.5/36.7	66.70/66.71	22.89/22.97	28.9/27.5	0.28	0.18	232	12	2.8	2.3	54.4	203.8
080922	14:30	8.3/7.9	67.86/67.87	23.53/23.57	26.0/27.5	0.21	0.32	63	19	0.6	1.2	18	189.4
081109	17:00	41.8/41.8	66.59/66.59	22.96/22.98	21.9/22.5	0.31	0.34	75	22	0.3	0.4	50.2	215
090129	22:20	35.4/34.9	69.01/69.04	23.79/23.77	33.1/37.5	0.28	0.37	109	21	0.4	0.3	22	233
090312	22:42	34.9/34.8	67.39/67.38	23.59/23.60	30.0/31.5	0.2	0.15	94	11	0.7	1.1	8.2	136.4

SED
7, 3689–3733, 2015

Table 4. Source parameters of selected events.

	Event 1 (shallow)	Event 2 (deep)
Date	13 Sep 2008	9 Nov 2008
Origin time (UTC)	07:21:10.7	17:00:41.8
Latitude (° N)	68.20	66.59
Longitude(° E)	23.79	22.96
Depth (km)	9.8	21.9
ML	1.9	2.0
1 Strike/dip/rake (deg)	199/84/−179	263/78/165
Fault plane uncertaintly (deg)	30	36
2 Strike/dip/rake (deg)	109/89/−6	356/75/12
Auxiliary plane uncertaintly (deg)	35	39
P axis: trend/plunge	64/5	310/2
T axis: trend/plunge	154/4	219/19

SED
7, 3689–3733, 2015

Table 5. Corrected by VELEST velocities in 2 and 3 layers, number of hypocentres NHYP in each layer and number of ray's trajectory passing through the layer NHIT.

Depth (km)	fllayer	Vp ($km\,s^{-1}$)	NHYP	NHIT
1.3–18.0	2	6.27	25	735
18–37	3	6.66	6	284

SED
7, 3689–3733, 2015

Table 6. Information about focal mechanisms of local earthquakes for Region 2 from other sources.

No.	data	Ml	depth	lat	lon	strike	dip	rake	Source
1	27 May 1987	2.0	14.0	66.64	22.37	30	80	34	(Arvidsson, 1996)
2	18 Jul 1987	2.4	34.0	66.42	21.71	205	70	20	(Arvidsson, 1996)
3	16 Nov 1989	1.6	12.5	68.83	23.67	0	90	0	(Bungum and Lindholm, 1996)
4	02 May 2001	2.9	5.0	67.16	24.59	35	30	90	(Uski et al., 2003)

SED
7, 3689–3733, 2015

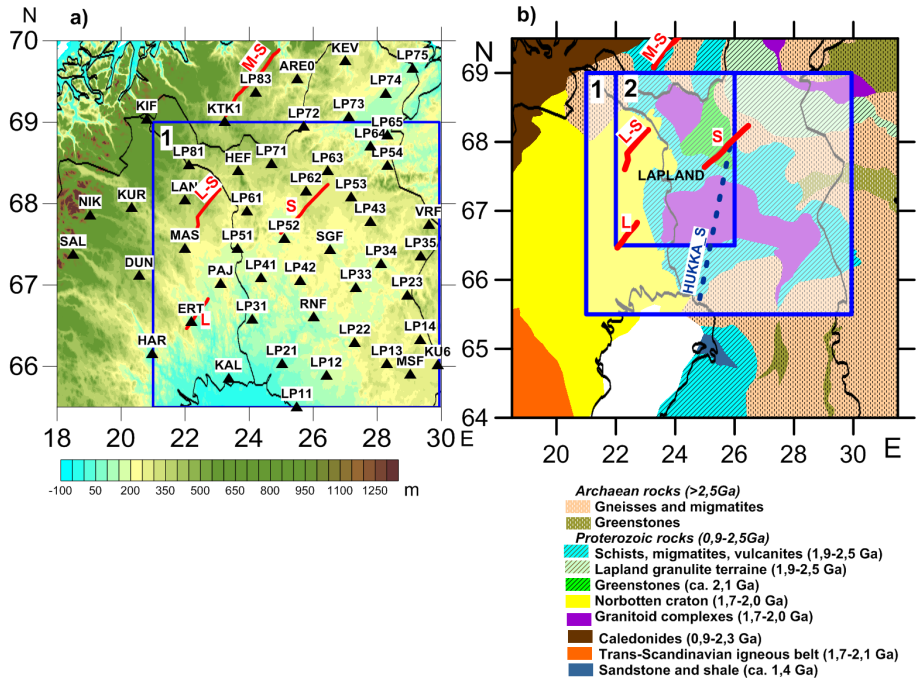

Figure 1. (a) Location of 56 POLENET/LAPNET stations (black triangles), imposed in topographic map ETOPO1 (Amante and Eakins, 2009, http://maps.ngdc.noaa.gov/viewers/wcs-client/), **(b)** The geological map, based on a 1 : 2 000 000 geological map of Fennoscandia (Koistinen et al., 2001). Red lines with letters (L, L-S, S, M-S) are denoted post-glacial faults (Muir Wood 1993): M-S – Mierujarvi–Sværholt Fault Zone, L-S – Lainio-Suljavaara, L – Lansjarv, S – Suasselka. Blue line – investigation Regions 1 and 2. Region 1 is the region for tomographic research and Region 2 is the region for reliable location. Blue dotted line – profile HUKKA S.

SED
7, 3689–3733, 2015

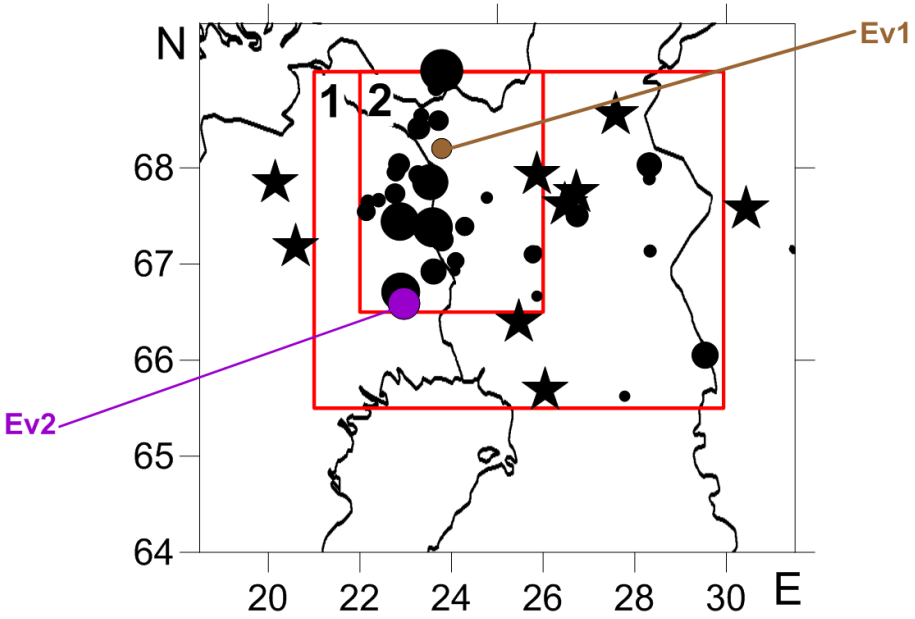

Figure 2. Epicentres of 36 local earthquakes (circles), 9 local explosions (stars), used in the study. Epicentres are given according to HEL catalogue. The size of circles is proportional to hypocentre depth. Ev1 and Ev2 – events from Table 4 with determined focal mechanisms.

SED
7, 3689–3733, 2015

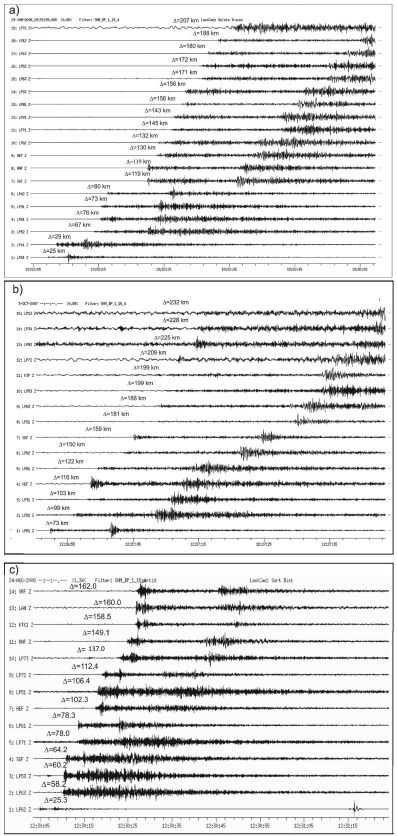

Figure 3. Examples of waveforms of local events in *Z* component: **(a)** shallow event 19 January 2008 19:52 UTC 67.23° N 23.80° E, depth = 10.4 km, ML = 2.2 (HEL), **(b)** deep event 3 October 2007 12:26 UTC 67.42° N 22.81° E, depth = 27.4 km, ML = 1.6 (HEL), **(c)** explosion in the Hukkavaara hill 24 August 2008 12:30 UTC 67.94° N 25.79° E, ML = 1.1 (HEL). Epicentral distances Δ were calculated using HEL catalogue.

SED
7, 3689–3733, 2015

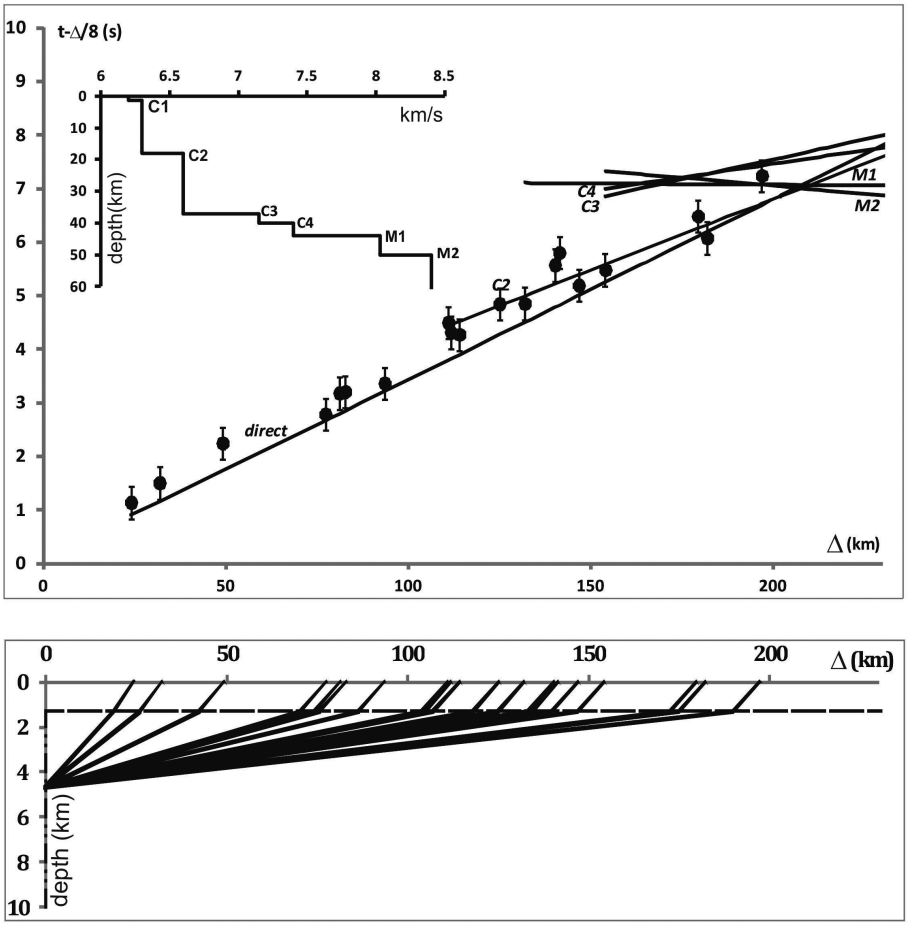

Figure 4. Ray propagation in 1-D layered model for shallow event. Lower panel: the rays through the model. Upper panel: the reduced calculated and picked travel times.

SED
7, 3689–3733, 2015

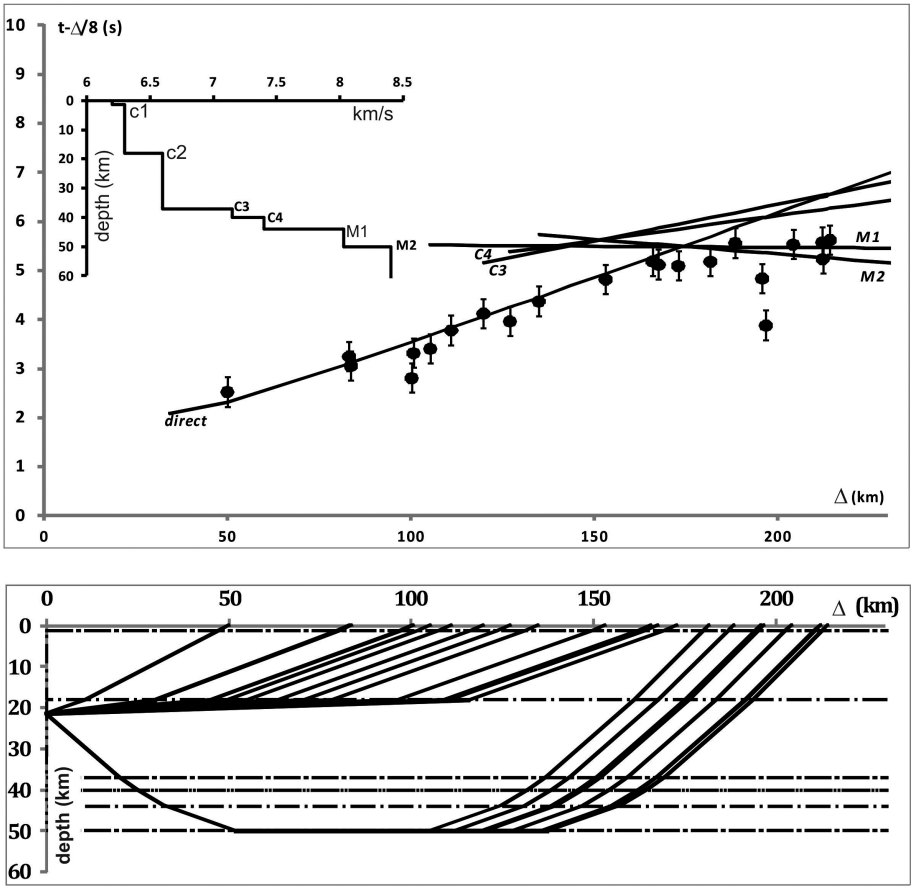

Figure 5. Ray propagation in 1-D layered model for deep event. Lower panel: the rays through the model. Upper panel: the reduced calculated and picked travel times.

SED
7, 3689–3733, 2015

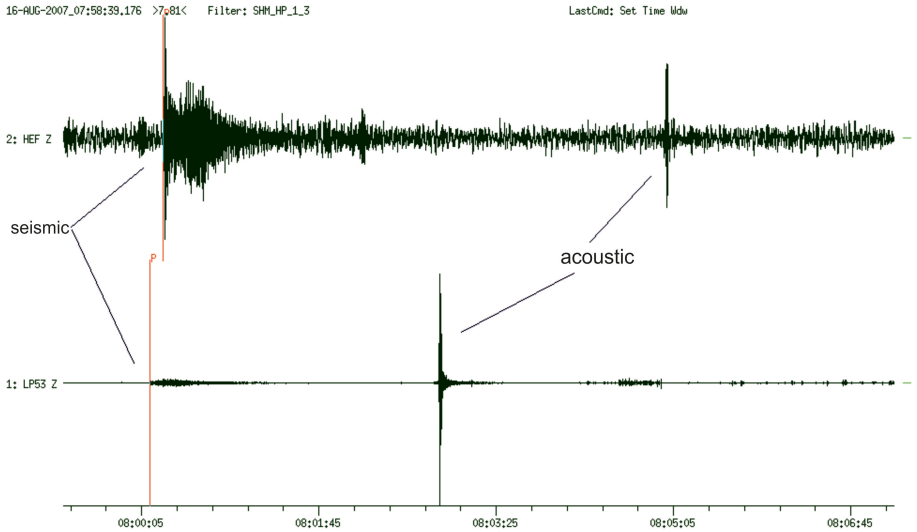

Figure 6. Seismograms of explosion 16 August 2007 08:00 UTC 67.93° N 25.82E ML = 1.5 (HEL) from Hukkavaara hill. Traces are normalized to maximum amplitude.

SED
7, 3689–3733, 2015

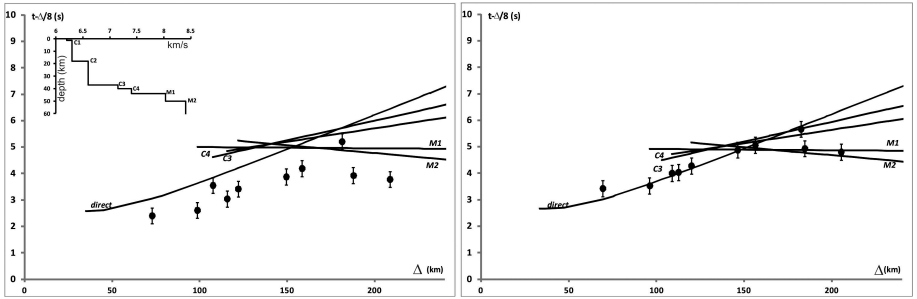

Figure 7. Result of relocation by HYPOELLIPSE: comparison of observed and calculated travel times for deep earthquake on 3 October 2007 12:26 UTC 67.42° N 22.81° E, depth = 27.4 km, ML = 1.6 (HEL). Left panel demonstrates travel times before relocation, right panel shows travel times after relocation.

SED
7, 3689–3733, 2015

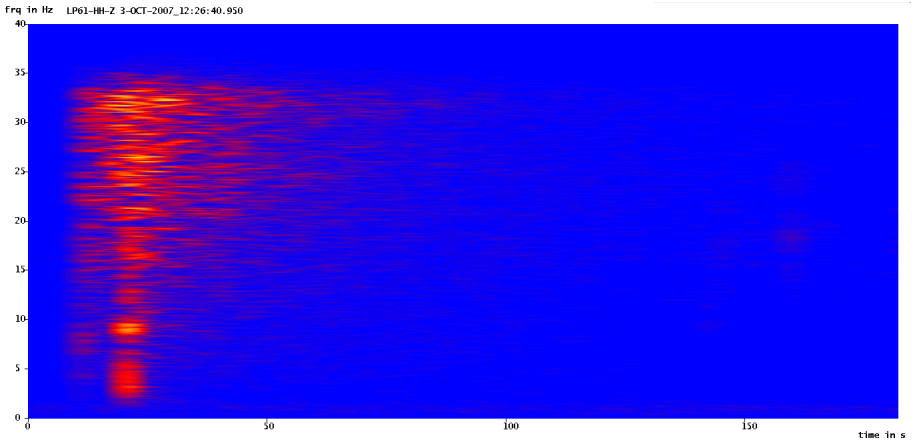

Figure 8. Spectrogram of deep earthquake on 3 October 2007 12:26 UTC 67.42° N 22.81° E, depth = 27.4 km, ML = 1.6 (HEL) on station LP61 (the offset equals 70 km).

SED
7, 3689–3733, 2015

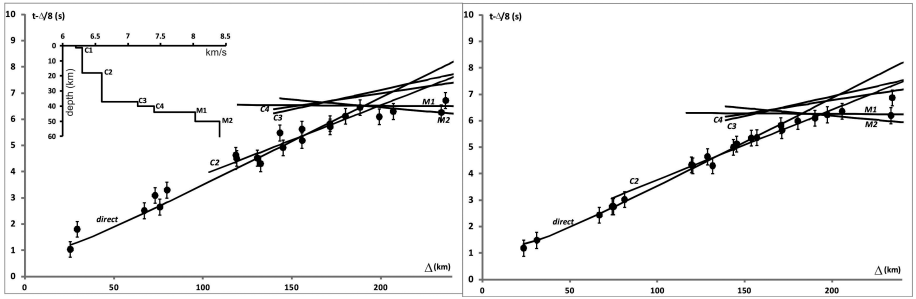

Figure 9. Result of relocation by HYPOELLIPSE: comparison of observed and calculated travel times for shallow earthquake 19 January 2008 19:52 UTC 67.23° N 23.80° E, depth = 10.4 km, ML = 2.2 (HEL). Left panel demonstrates travel times before relocation, right panel shows travel times after relocation.

SED
7, 3689–3733, 2015

Figure 10. Seismograms for shallow event Ev1 from Table 4 showing the first motions for different resampling: **(a)** 50 Hz, **(b)** 80 Hz **(c)** 100 Hz. The traces are aligned relatively to the first *P* arrival.

SED
7, 3689–3733, 2015

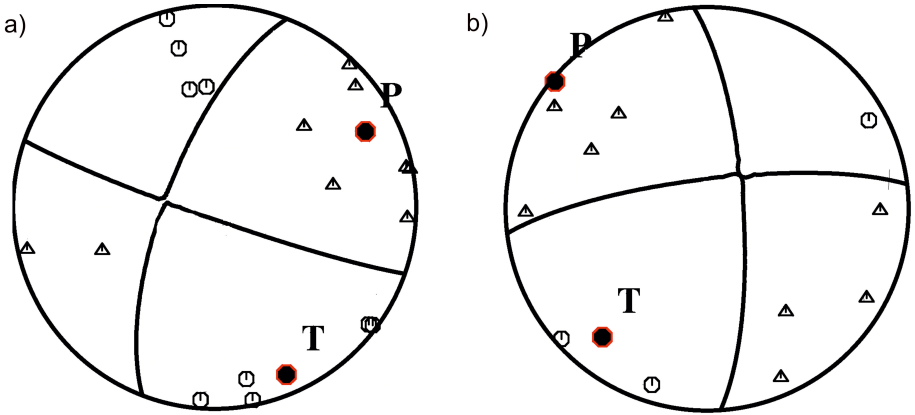

Figure 11. Lower hemisphere equal area projections of the focal sphere for **(a)** Ev 1 (shallow) and **(b)** Ev 2 (deep). For the polarities, octagons and triangles represent compressions and dilatations. Letter symbols indicate the position of compressional (*P*) and tensional (*T*) axes.

SED
7, 3689–3733, 2015

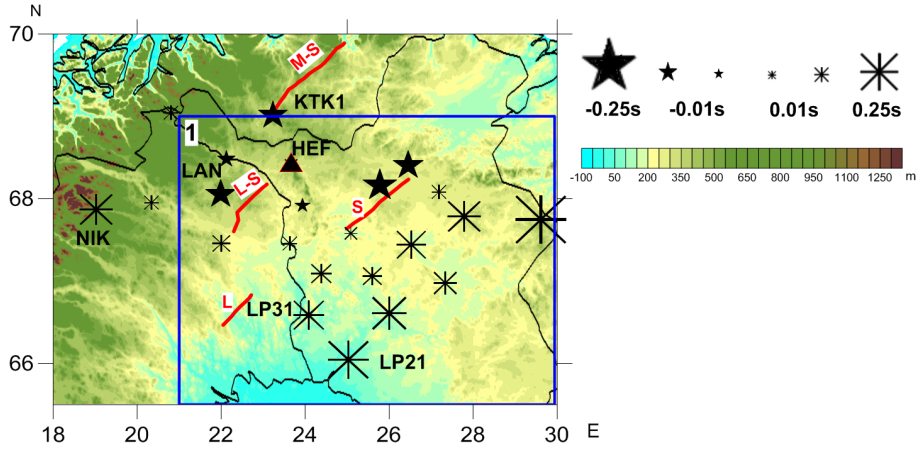

Figure 12. The time station corrections imposed in topographic map ETOPO1 (Amante and Eakins, 2009) and computed with respect to the reference station HEF by VELEST. Stars are denoted negative corrections, snowflakes are denoted positive corrections. The size of the sign (star or snowflake) is proportional to value of correction. The red lines with letters (L, L-S, S, M-S) are denoting post-glacial faults (Muir Wood, 1993). Blue line indicates investigation Region 1. The full names of faults are the same as in Fig. 1b.

SED
7, 3689–3733, 2015

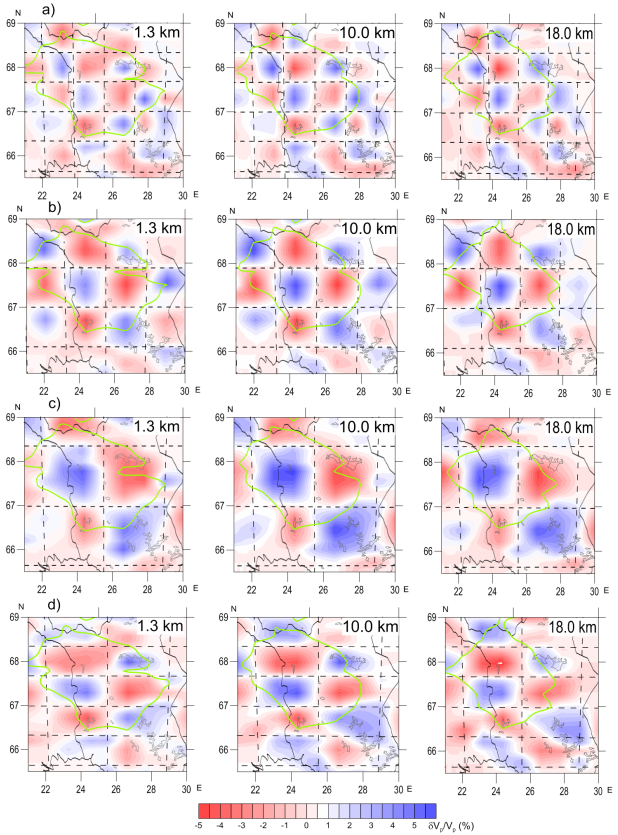

Figure 13. Results of the checkerboard test for checks **(a)** 75 km × 75 km, **(b)** 100 km × 100 km, **(c)** 150 km × 150 km, **(d)** 150 km × 75 km. Horizontal cross sections of the reconstructed pattern are shown for depths 1.3, 10.0 and 18.0 km. The dotted lines are the boundaries of synthetic checks with different velocity in testing model. Green contour restrict the area with resolution more than 0.5.

SED
7, 3689–3733, 2015

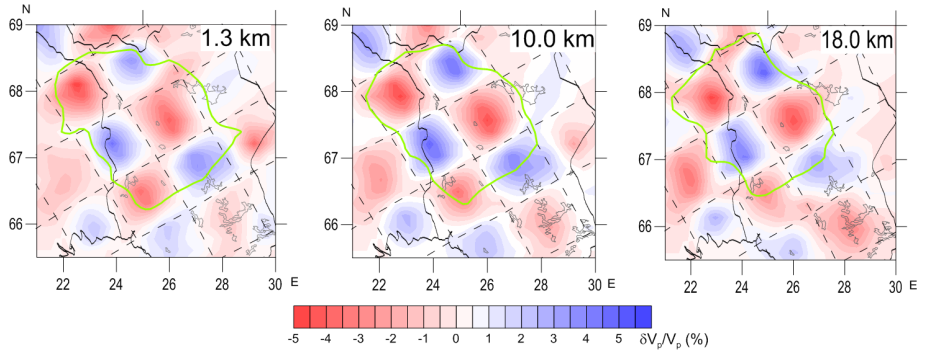

Figure 14. Results of synthetic checkerboard test for checks of 100 km × 100 km, oriented at angle of 30° counter clockwise from the North. The other descriptions are the same as in Fig. 13.

SED
7, 3689–3733, 2015

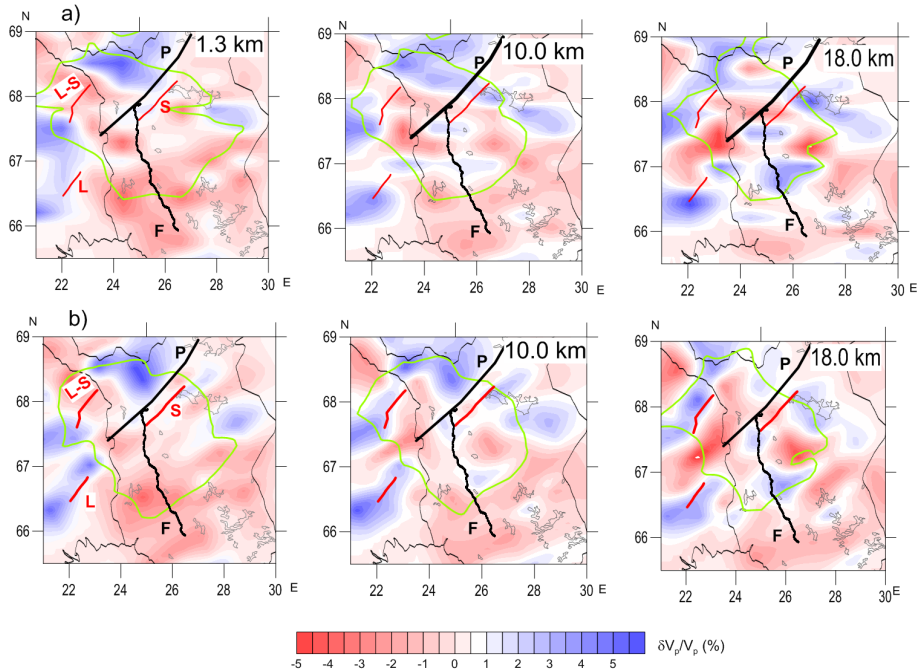

Figure 15. Upper crustal 3-D velocity structure of the Region 1 reconstructed with SIMULPS14. Horizontal cross sections for depths: 1.3, 10.0, 18.0 km **(a)** for usual grid, **(b)** for grid, oriented at angle of 30° counter clockwise from the North. Green contour restrict the area with resolution more than 0.5. Red lines (in Sect. 1.3 km with letters L, L-S, S) are denoted post-glacial faults (Muir Wood, 1993) (detailed in Fig. 1). Black lines are denoted profiles: FIRE with letter F, POLAR with letter P.

SED
7, 3689–3733, 2015

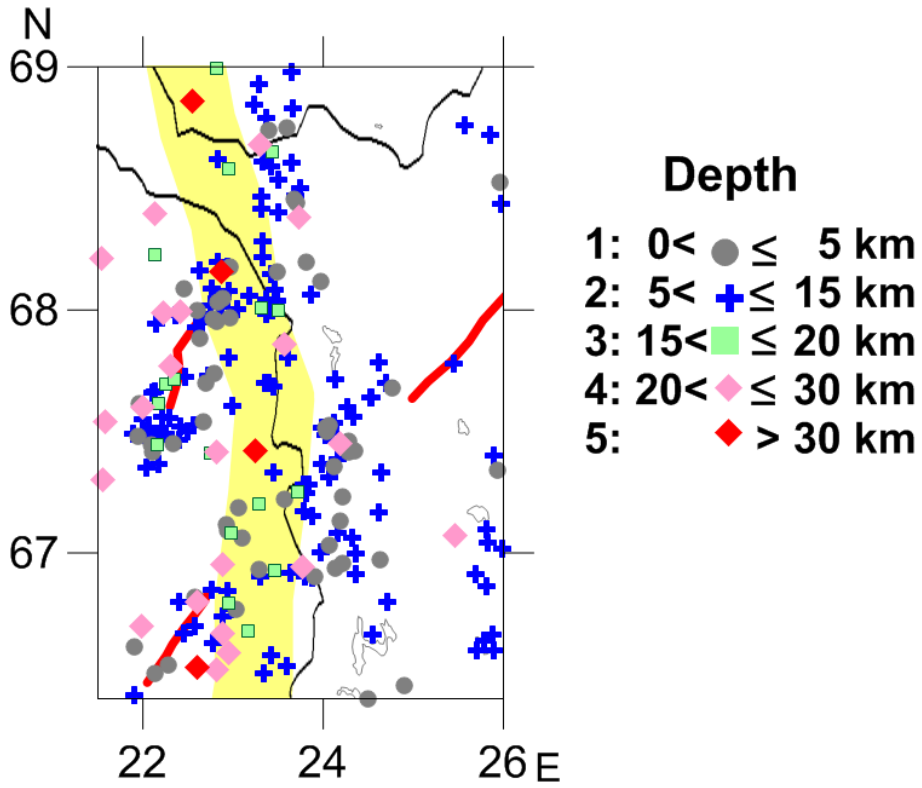

Figure 16. Local earthquakes from catalogue HEL in the period with 1964 to 2008 years in the Region 2. The earthquakes are divided in 5 groups depending on hypocentre depth. The number of earthquakes equals 55 in 1 group, 126 in 2 group, 17 in 3 group, 21 in 4 group, 4 in 5 group. Red lines are denoting post-glacial faults. Baltic–Bothnia Megashear (BBMS) from (Berthelsen and Marker, 1986) is shown by yellow stripe.

SED
7, 3689–3733, 2015

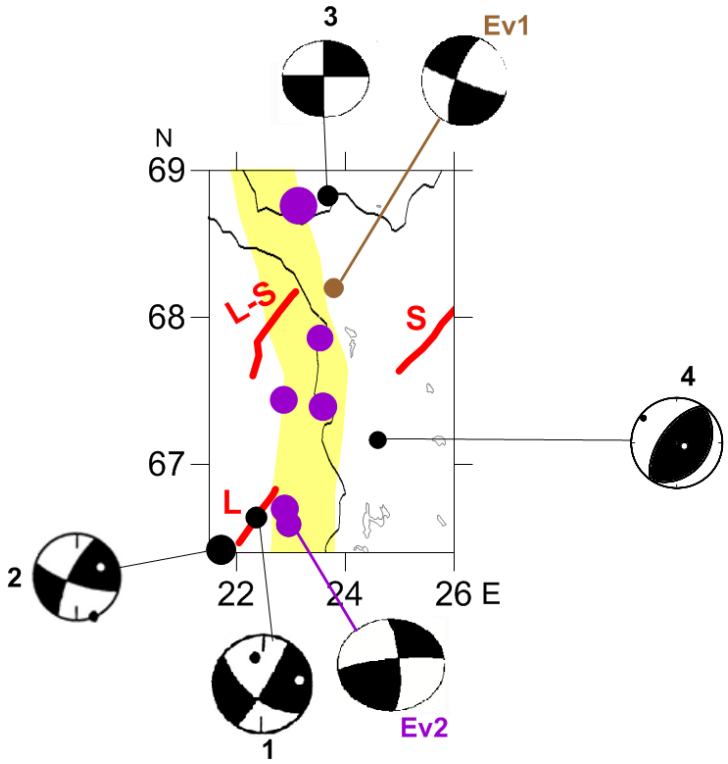

Figure 17. Available fault plane solutions for the earthquakes in Region 2 (lower hemisphere equal area projection): black circles show events from Table 6. Deep earthquakes with reliable location from Table 3 are shown by purple circles. Events for which we calculated focal mechanisms (Table 4) are indicated by brown circle (shallow one) and purple circle (deep one). The size of circles is proportional to the depth of event. Red lines with letters are denoting post-glacial faults (details in Fig. 1). BBMS from (Berthelsen and Marker, 1986) is shown by yellow stripe.

SED
7, 3689–3733, 2015